Isolation, Semisynthesis, Covalent Docking and Transforming Growth Factor Beta-Activated Kinase 1 (TAK1)-Inhibitory Activities of (5Z)-7-Oxozeaenol Analogues

By: Lara Fakhouri, Tamam El-Elimat, Dow P. Hurst, Patricia H. Reggio, Cedric J. Pearce, Nicholas H. Oberlies, and Mitchell P. Croatt

"Isolation, Semisynthesis, Covalent Docking and Transforming Growth Factor Beta-Activated Kinase 1 (TAK1)-Inhibitory Activities of (5Z)-7-Oxozeaenol Analogues." Lara Fakhouri, Tamam El-Elimat, Dow P. Hurst, Patricia H. Reggio, Cedric J. Pearce, Nicholas H. Oberlies, and Mitchell P. Croatt. *Bioorganic & Medicinal Chemistry, 2015, 23*(21), 6993-6999. PMID: 26481152; PMCID: PMC4661079; doi: 10.1016/j.bmc.2015.09.037

Made available courtesy of Elsevier: https://doi.org/10.1016/j.bmc.2015.09.037

Abstract:

(5*Z*)-7-Oxozeanol and related analogues were isolated and screened to explore their activity as TAK1 inhibitors. Seven analogues were synthesized and more than a score of natural products isolated that examined the role that different areas of the molecule contribute to TAK1 inhibition. A novel nonaromatic difluoro-derivative was synthesized that had similar potency compared to the lead. This is the first example of a nonaromatic compound in this class to have TAK1 inhibition. Covalent docking for the isolated and synthesized analogues was carried out and found a strong correlation between the observed activities and the calculated binding.

Keywords: (5Z)-7-Oxozeaenol | TAK1 | Selectfluor® | Covalent docking | Resorcylic acid lactone

Article:

1. Introduction

Transforming growth factor-β-activated kinase 1 (TAK1) is a member of the serine/threonine mitogen-activated protein kinase kinase kinase (MAP3K) family.[1] A wide range of extracellular stimuli, such as proinflammatory interleukins, activate the intracellular TAK1 via membrane-bound receptors.[2] Turning on of the upstream key signaling enzyme results in subsequent phosphorylation of specific MAP2Ks and MAPKs, which in turn activates a number of transcription factors including AP-1 and NF-κB.[3] The aforementioned DNA-binding proteins are known to regulate inflammatory responses and apoptosis. Inhibition of upstream kinases such as MAP3Ks has an advantage over inhibiting downstream signaling molecules, mostly due to the

former being more stimuli-specific.[4] Indeed, it has been shown that inhibiting the TAK1/NF-κB signaling pathway, using either TAK1 inhibitors or via silencing its expression, promotes apoptosis in colon cancer,[5] suppresses renal cell[6] carcinoma survival,[7] inhibits proliferation of LPS-induced human hepatocellular carcinoma,[8] and reverses chemoresistance of pancreatic cancer.[9]

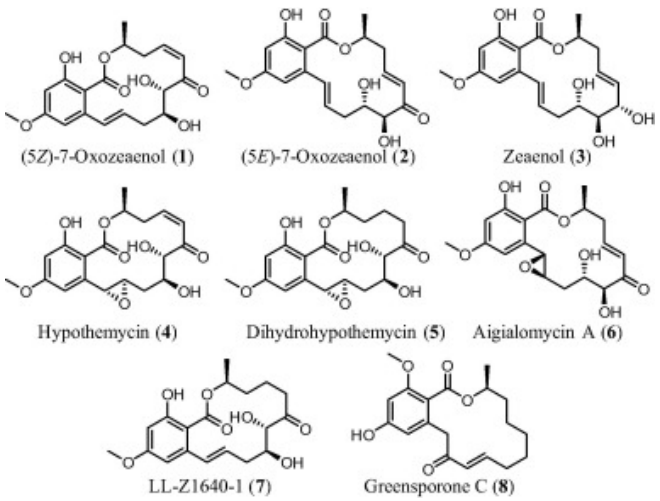

Figure 1. Structures of isolated RALs from MSX 63935 (**1**–**7**) and a representative RAL from a different fungal strain (see Fig. S19 for additional isolated compounds).

In 1978, Ellestad et al. reported the isolation of (5*Z*)-7-oxozeaenol (**1**) (Fig. 1), a β-resorcylic acid lactone (RAL), from an unidentified fungus.[10] (5*Z*)-7-Oxozeaenol and its synthetic derivatives have received extensive attention for their biological activities.[11] In 2003 it was found that **1** was a potent inhibitor of TAK1 with an IC_{50} of 8.1 nM.[12] (5*Z*)-7-Oxozeaenol binds covalently to its target and, similar to almost all other kinase inhibitors,[13] is a competitive ATP ligand that binds covalently to its target.[12] This irreversible interaction was determined when the covalently-bound ligand was co-crystalized with TAK1.[14] The interest in discovering and developing small molecule covalent inhibitors stems from the fact that these ligands may have increased selectivity for their targets and therefore the potential for less intense side effects, resulting from dose reduction of the candidate drug to achieve therapeutic efficacy.[15] Selectivity of covalent inhibitors between kinases is difficult to achieve because the target is the ATP-binding pocket, which is highly conserved.[16] However, the selectivity profile often improves when moving from biochemical to cell-based kinase screening. There was a promising degree of selectivity for (5*Z*)-7-oxozeaenol since a 1 μM concentration exhibited at least 50% inhibition for only 12 of the 85 kinases tested by Wu et al. and in cell lines the macrolide inhibitor was even more selective for TAK1 inhibition.[14] Due to the selective and potent activity with this medicinally important receptor, it was decided that (5*Z*)-7-oxozeaenol was worth further analysis. Filamentous fungus MSX 63935 is a prolific producer of (5*Z*)-7-oxozeaenol, reproducibly biosynthesizing over 800 mg per a single solid-based culture grown in a 2.8 L Fernbach flask.[17] Six structurally related analogues of **1** were concomitantly isolated from this fungus (Fig. 1, **2**–**7**) and 16 compounds from other strains (**8** and S1–S15; see SI for full listing of structures).[18] Seven additional compounds were also produced by semisynthesis using (5*Z*)-7-oxozeaenol as the starting material (Scheme 1). All 30 compounds were analyzed for their inhibitory activity with TAK1. Covalent docking of the isolated and synthesized analogues was

carried out to correlate, at a molecular level, structural changes with variations in inhibitory activity. These data are herein presented to establish structure–activity relationships for (5*Z*)-7-oxozeaenol's TAK1 activity.

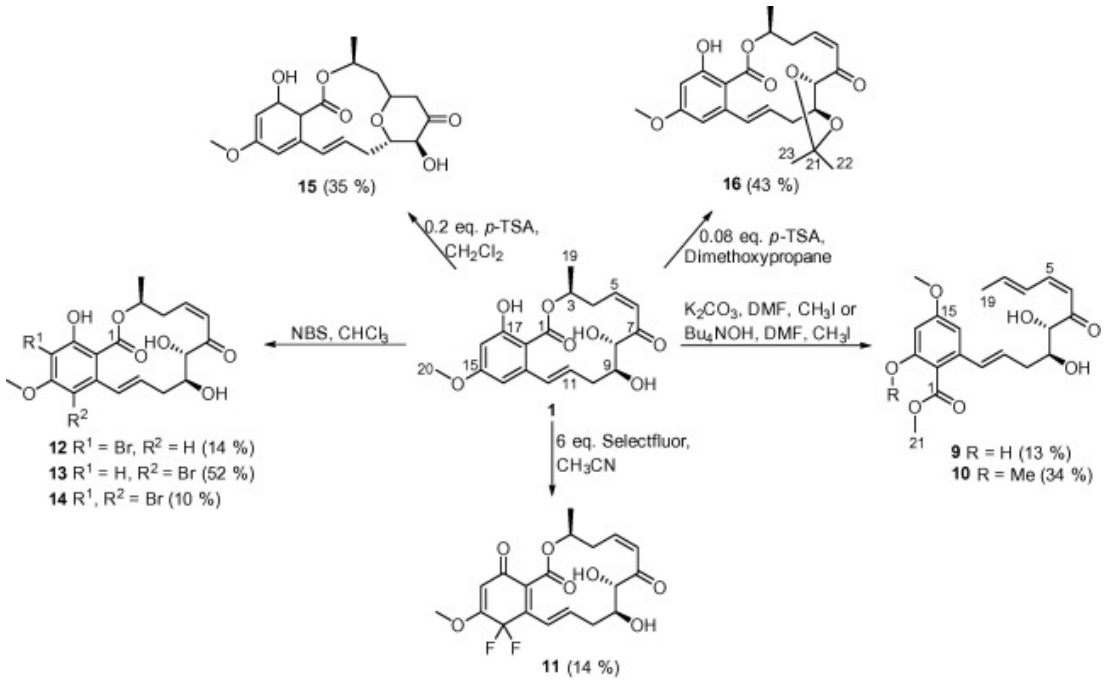

Scheme 1. Synthesis of compounds **9**–**16**.

2. Results and discussion

2.1. Isolation of (5*Z*)-7-oxozeaenol (**1**) and related secondary metabolites

The lead compound in this study, (5*Z*)-7-oxozeaenol **1**, and six related analogues (Fig. 1) were isolated from solid-phase cultures of MSX 63935 as previously described in detail.[17] The decision of choosing **1** as the lead for further diversification was primarily due to the greater potency in inhibiting NF-κB (11 nM).[17] Fortuitously, the relative amount of *cis*-enone **1** was much higher in the extract compared to all other metabolites.[17] In addition to the seven compounds from MSX 63935, 14 structurally related compounds were isolated from natural sources as previously described.[16]

2.2. Synthesis of (5*Z*)-7-oxozeaenol analogues

The rationale for analogue design was to explore key areas of the pharmacophore of (5*Z*)-7-oxozeaenol. The free phenol was the first appealing position to synthetically diversify. The main reason for methylating the phenol was to verify the prior hypothesis that the phenol hydrogen bonds to the carbonyl of nearby residue Pro160.[14] The use of diazomethane[19] or iodomethane with sodium hydride[20] did not result in the methylation of the hydroxy at carbon 17, as indicated by ^{1}H NMR spectroscopy. Instead, macrolactone **1**either decomposed or was unreactive under those conditions. The phenolic hydrogen is strongly hydrogen bonded to the nearby ester carbonyl oxygen, as can be inferred from the sharp singlet at 12 ppm in ^{1}H NMR spectrum of **1**.

The use of potassium carbonate[21] or tetrabutylammonium hydroxide[22] in DMF produced a reaction, but only elimination instead of substitution (Scheme 1). Dienoates **9** and **10** suggest that the strong bases deprotonated one of the hydrogens on carbon 3 and this led to elimination of the ester attached to carbon 3. Under these more forcing conditions, the phenol was found to react with excess iodomethane. The stereochemical configurations of compounds **9** and **10** were assigned as (3*E*,5*Z*) based on the coupling constants between the protons at C3/C4 and C5/C6 (i.e., 13.8 Hz and 11.5 Hz, respectively). Although dienoate **9** could be characterized, it was not sufficiently stable to be examined for biological activity.

There has been an increased interest in introducing fluorine atoms into drug candidates for the enhanced pharmacokinetics and pharmacodynamics that this atom provides. For example, more than 25% of marketed drugs have at least one fluorine atom in their structures.[23] The small size and large electronegativity of this heteroatom often leads to an increase in drug potency and half-life due to decreased metabolism. In light of these advantages, fluorination was attempted. The reagent of choice for this reaction was the electrophilic Selectfluor®, which usually has high levels of reactivity and selectivity.[24] Surprisingly, the product obtained was a result of difluorination at carbon 14 (Scheme 1). Attempts to synthesize the monofluorinated compound led only to reduced yields of the difluorinated product. Although this difluoro compound (**11**) was unexpected, it is highly important since it tests hydrogen bond donation at the phenolic position and is the first nonaromatic structure in the class of molecules to be tested for binding to TAK1.

In a separate attempt to introduce fluorine into the molecule, trifluoromethylation was carried out. Unexpectedly, the major product obtained when using sodium trifluoromethane sulfinate, copper(II) trifluoromethane sulfonate and hydrogen peroxide[25] resulted in the formation of bromide **12** (Scheme 1). It was surmised that trace impurities of a bromine-containing contaminant, as suggested by mass analysis of sodium trifluoromethane sulfinate, were the source of reactive bromine. Fortunately, when arene **1** was treated with NBS, bromination at either or at both positions occurred to provide for more reproducible bromination conditions.[26]

To investigate the importance of the free hydroxyl groups at carbons 8 and 9 for activity, acetonide formation was targeted. The use of acetone with dimethylsulfoxide[27] was not successful to prepare the target product, however, dimethoxypropane with catalytic amounts of *p*-toluenesulfonic acid was successful if only 0.08 equiv[10] of the acid were used. Larger amounts of acid[28] in CH_2Cl_2 activated the carbonyl at carbon 7 and facilitated intramolecular conjugate addition of the oxygen at carbon 9 to give pyranone **15** (Scheme 1).

2.3. Analysis of TAK1 inhibition

The synthesized analogues **10**–**16**, isolated RALs **1**–**8** (Fig. 1), and RALs **S1**–**S15** (Fig. S19) were evaluated for their in vitro TAK1 inhibitory activities (Table 1). Compound **9** was not tested due to the short term stability as indicated by the sub 90% purity detected by UPLC following prep HPLC purification. It was verified that the Michael acceptor was, as expected, a crucial part for the inhibitory activity of this group of compounds. Loss of this functionality, which is involved in covalent bond formation, whether through reduction of the double bond or reduction of the carbonyl, lead to loss of activity as seen with zeaenol (**3**), LL-Z164-1 (**7**),

dihydrohypothemycin (**5**), pyranone **15**, and compounds **S1**–**S15**. Not only was the enone presence crucial to the pharmacophore structure, the position matters also, since shifting the enone from $\Delta^{5,7}$ to $\Delta^{9,11}$, as in greensborone C (**8**), diminished activity. Additionally, isomerization of the enone double bond from a *Z* to an *E* configuration significantly reduced activity. This effect can be seen comparing two different pairs of isomers, namely; (5*Z*)-7-oxozeaenol (**1**) versus (5*E*)-7-oxozeaenol (**2**) and hypothemycin (**4**) versus aigialomycin A (**6**).

Table 1. Docking scores of enone-containing natural and semisynthetic RALs following prime minimization

Structure	Docking score	IC_{50}[a] (μM)
1	−12.9	0.011
4	−12.0	0.033
11	−12.9	0.077
13	−10.2	0.36
16	−10.8	0.38
6	N/A[b]	0.99
2	−11.5	1.3
12	−10.0	2.6
7	N/A[b]	2.6
14	−6.8	8.9
3	N/A[b]	10
5	N/A[b]	>30
8	−8.4	>30
10	−6.4	>30
15	N/A[b]	>30

[a] See Table S1 for the 95% confidence intervals.
[b] Compounds were not docked due to a lack of a suitable Michael acceptor functionality.

By comparing **1** and **4**, it can be inferred that epoxidation of the double bond on carbons 11 and 12 does not change the inhibitory activity. As mentioned by Chen et al.[14], the hydroxy group located at carbon 9 binds to the enzyme via formation of a hydrogen bond with the backbone carbonyl of Pro160. As expected, blocking this interaction, as seen in acetonide **16**, reduced the activity by more than 30 fold. The inability of compound **10** to inhibit TAK1 indicated that the macrocycle was important for activity, probably due to the rigidity it provides to correctly position the Michael acceptor close to the nucleophilic cysteine residue. The only derivatized analogue that was found to be statistically equipotent to **1**was difluoro (5*Z*)-7-oxozeaenol **11**. The relative potency of **11** indicated that the aromatic ring was not crucial for binding. This observation with TAK1 and related structures is unprecedented.

The crystal structure of **1** bound to TAK1 indicated that there was insufficient space to accommodate a bromine atom on carbon 16. Thus, as expected, the 16-bromo analogue (**12**) was significantly less active. As for substituting position 14 with bromine; the aforementioned analogue **13** showed better activity than **12**, yet was 5 times less active than the difluoro derivative **11**, despite the fact that the radius of bromine atom is almost equivalent to two fluorine atoms. A possible explanation of such difference between **11** and **13** is attributed to the observation, shown in the covalent docking outputs of the two ligands, that the two fluorines were oriented deeper into the binding pocket, while the bromine protrudes further out of the binding pocket, creating unfavorable interactions with residues 42, 43 and 111. Alternatively, the electronic nature of the six-membered ring is also significantly altered between the difluoro

compound (**11**) and the 14-bromo compound (**13**), which could also impact binding. The added clashes of having bromine at positions 14 and 16 rendered dibromo analogue **14** the least active.

2.4. Covalent docking

Prior to docking, ligands having the Michael acceptor moiety were examined using Spartan (Wavefunction, Inc.).[29] Compounds without the Michael acceptor were not suitable for this covalent docking study since the cysteine needs to covalently add into the compound. The structures of those ligands were first subjected to conformational searches using semiempirical molecular mechanics. The resulting conformers, ranging from 100 to 600, were further optimized using Hartree–Fock implementing the 6-31G* basis set. The theoretical global minimum energy conformation was chosen to be docked into the crystal structure.

The prepared ligands were docked using the Chen and co-workers[14] reported crystal structure (PDB 4GS6). The crystal structure was first prepared using protein preparation wizard (Maestro), and the prepared ligands were docked using covalent docking implemented in Maestro.

To validate the accuracy of the calculations performed in regards to our work, (5*Z*)-7-oxozeaenol **1** was the first ligand docked and the output was superimposed to the crystal structure having an RMSD of 0.0984 Å (Fig. 2). The geometry shown in the crystal structure was that of sp^2 carbons at carbons 5 and 6. It is assumed that the geometry of carbons 5 and 6 in the crystal structure were incorrectly assigned, since both of these carbons should be sp^3 hybridized after addition of the cysteine. After overlaying the two possible options (*R* and *S* at carbon 5), it was determined that the 5*S*-diastereomer was a better fit, especially with the cysteine in the crystal structure. We therefore hypothesize that the crystal structure should actually be 5*S*.

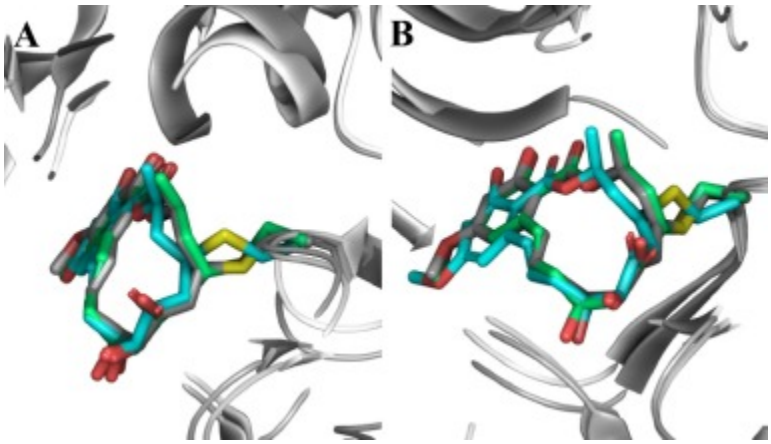

Figure 2. (A) Superimposed covalent docking output pose for the 5*R* (blue) and 5*S* (green) diastereomers with the cocrystalized (5*Z*)-7-oxozeaenol (gray). Parts of the enzyme's residues (R44, G45, A46, Y106, A107 and E108), in the binding pocket, were deleted for clarification; (B) −90° rotation of (A) around *Y* axis. Deleted enzyme residues are D175, F176 and G177.

Similar to the parent ligand, semisynthesized and isolated RALs bearing an enone were also docked covalently. The best docking orientations, as judged by the docking score, were further subjected to protein refinement using prime implemented in Maestro followed by covalent docking of the minimization outputs (Table 1). Distinct gaps were observed between compounds

having inhibitory concentrations in the nM range, low μM range, and the inactive compounds. Analogues having low nM inhibitory concentration had docking scores of −12 to −12.9 Kcal/mol. A range of −10 to −11.5 Kcal/mol was representative of analogues having 0.4–2.6 μM range of activities. Inactive compounds had considerably worse docking scores compared with the active compounds.

3. Conclusion

(5*Z*)-7-Oxozeaenol (**1**) and twenty-nine diverse analogues were isolated and synthesized to examine their potential medicinal value as TAK1 inhibitors. It was determined that the presence, position, and stereochemical configuration of the Michael acceptor was of importance, along with the presence of the macrolactone. A nonaromatic difluorocyclohexenone was found to have only a moderate reduction in activity, which is of significance since all prior structures examined that are related to this scaffold had the aromatic ring. Bromination of two positions of the aromatic ring was explored and it was determined that a bromine in the 16 position was highly detrimental, whereas a bromine in the 14 position was tolerated. A covalent docking model, based on the previously reported crystal structure,[12] was utilized to rationalize the activities. The modeling was also explored to formulate a hypothesis about the correct diastereomer of the covalently bound ligand since the reported crystal structure is lacking this stereochemical information. Future studies into metabolic stability and selectivity of these analogues are underway.

4. Experimental

4.1. General experimental procedures

All solvents and reagents were obtained from commercial sources and were used as received. The purification of **1** from solid state cultures of MSX 63935 was performed as has been previously described.[17] Unless otherwise stated, all reactions were carried out under an atmosphere of dry nitrogen in dried glassware. Indicated reaction temperatures refer to those of the reaction bath, while room temperature (rt) is noted as 25 °C. Analytical thin layer chromatography (TLC) was performed on silica gel 60 F254 precoated plates (0.25 mm) from Merck. Visualization was accomplished by irradiation under a 254 nm UV lamp. Silicycle silica gel 230–400 (particle size 40–63 μm) mesh was used for all flash column chromatography. The crude extract and reaction products were purified by reverse phase chromatography, which was performed using a Varian purification system employing a Phenomenex Gemini-NX, (5 μm, C18, 110A, AX. 250 × 21.20 mm). The mobile phase was a mixture of acetonitrile and H_2O containing 0.1% formic acid. ^{1}H NMR spectra were recorded on a JEOL ECA 500 MHz spectrometer or a JEOL ECS 400 MHz spectrometer in the solvent indicated. All ^{1}H NMR experiments are reported in δ units, parts per million (ppm) downfield of TMS, and were measured relative to the signals for chloroform (7.26 ppm), methanol (3.31 ppm), acetone (2.05 ppm) and dimethylsulfoxide (2.50 ppm). All ^{13}C NMR spectra were reported in ppm relative to the signals for chloroform (77.0 ppm), methanol (49.0 ppm), acetone (29.8 ppm) and dimethylsulfoxide (39.5 ppm) with ^{1}H decoupled observation. Data for ^{1}H NMR are reported as follows: chemical shift (δ ppm), multiplicity (s = singlet, d = doublet, t = triplet, q = quartet, quint = quintet, sext = sextet, sept = septet, m = multiplet, bs = broad singlet), integration and

coupling constant (Hz), whereas ^{13}C NMR analyses were reported in terms of chemical shift. High resolution mass spectra (HRMS) were performed on a Thermo Fisher Scientific UPLC/LTQ Orbitrap XL system.

4.2. Synthesis of (5*Z*)-7-oxozeaenol analogues

4.2.1. Methyl 2-((1*E*,4*S*,5*S*,7*Z*,9*Z*)-4,5-dihydroxy-6-oxoundeca-1,7,9-trien-1-yl)-6-hydroxy-4-methoxybenzoate (**9**)[21]

Potassium carbonate (38 mg, 0.28 mmol) was added to a solution of (5*Z*)-7-oxozeaenol (50 mg, 0.14 mmol) in DMF (2 mL) and stirred for an hour at rt. Iodomethane (10 µL, 0.16 mmol) was then added and the mixture stirred for 4 h at rt. It was diluted with water (20 mL) and acidified with 1 M HCl to pH of 2, followed by extraction with $CHCl_3$(20 mL × 3). The combined organic layers were dried using anhydrous sodium sulfate and the solvent evaporated. The residue was purified by preparative HPLC using a Phenomenex Gemini-NX column C18 (250 × 21.20 mm, 110 A, 5 µm spherical particle size). The column was perfused at a flow rate of 21.24 mL/min with 70% of (water, 0.1% FA) and 30% of (CH_3CN) over 80 min. The compound eluted at ~70 min. Yield (6.6 mg, 13%). ^1H NMR (500 MHz, $CDCl_3$) δ 11.56 (s, 1H; 17-OH), 7.43 (ddq, J_q = 1.2 Hz, J_d = 11.5, 14.9 Hz, 1H; 4-H), 6.98 (d, J = 15.5 Hz, 1H; 12-H), 6.57 (dd, J = 11.2, 11.5 Hz, 1H; 5-H), 6.41 (d, J = 2.9 Hz, 1H; 14-H), 6.37 (d, J = 2.9 Hz, 1H; 16-H), 6.25 (dq, J_d = 14.9 Hz, J_q = 6.9 Hz, 1H; 3-H), 6.08 (d, J = 11.5 Hz, 1H; 6-H), 5.84 (dt, J_d = 15.5 Hz, J_t = 7.5 Hz, 1H; 11-H), 4.37 (bs, 1H; 8-H), 3.95 (dt, J_t = 4.6 Hz, J_d = 8.0 Hz, 1H; 9-H), 3.91 (s, 3H; 21-H), 3.80 (s, 3H; 20-H), 2.33–2.40 (m, 2H; 10-H), 1.90 (d, J = 6.9 Hz, 3H; 19-H). ^{13}C NMR (125 MHz, $CDCl_3$) δ 198.9, 171.5, 164.9, 164.2, 146.7, 145.2, 142.8, 135.2, 129.3, 127.5, 117.9, 108.5, 103.7, 100.0, 79.4, 72.2, 55.5, 52.3, 35.7, 19.0. HRMS (ESI, *m*/*z*): Calculated for $C_{20}H_{25}O_7$ $[M+H]^+$ 377.1595; found 377.1589 (1.5 ppm).

4.2.2. Methyl 2-((1*E*,4*S*,5*S*,7*Z*,9*Z*)-4,5-dihydroxy-6-oxoundeca-1,7,9-trien-1-yl)-4,6-dimethoxybenzoate (**10**)[21]

Same as procedure described for synthesis of compound **9**. Compound **10** eluted at ~46 min. UPLC was used to evaluate the purity using a gradient solvent system that initiated with 20:80 CH_3CN−H_2O to 100% CH_3CN over 4.5 min (>97% pure; Fig. S1, SI). Yield (18.0 mg, 34%). ^1H NMR (500 MHz, $CDCl_3$) δ 7.43 (ddq, J_q = 1.2 Hz, J_d = 11.5, 14.9 Hz, 1H; 4-H), 6.57 (d, J = 11.5 Hz, 1H; 5-H), 6.54 (d, J = 2.3 Hz, 1H; 14-H), 6.40 (d, J = 15.8 Hz, 1H; 12-H), 6.34 (d, J = 2.3 Hz, 1H; 16-H), 6.24 (dq, J_d = 14.9 Hz, J_q = 6.9 Hz, 1H; 3-H), 6.13 (dt, J_d = 15.8 Hz, J_t = 7.5 Hz, 1H; 11-H), 6.04 (d, J = 11.5 Hz, 1H; 6-H), 4.35 (d, J = 4.0 Hz, 1H; 8-H), 3.96–3.92 (m, 1H; 9-H), 3.87 (s, 3H; 21-H), 3.80 (s, 3H; 22-H), 3.78 (s, 3H; 20-H), 2.42–2.35 (m, 1H; 10-H), 2.26 (ddd, J = 4.0, 7.4, 14.3 Hz, 1H; 10-H), 1.89 (d, J = 6.9 Hz, 3H; 19-H). ^{13}C NMR (125 MHz, $CDCl_3$) δ 198.8, 168.7, 161.6, 158.2, 146.9, 145.2, 137.8, 130.5, 129.4, 129.3, 117.9, 115.3, 101.8, 97.9, 79.4, 72.4, 56.1, 55.5, 52.5, 35.9, 19.1. HRMS: (ESI, *m*/*z*): Calculated for $C_{21}H_{27}O_7$ $[M+H]^+$ 391.1751; found 391.1745 (1.6 ppm).

4.2.3. (3*S*,5*Z*,8*S*,9*S*,11*E*)-13,13-Difluoro-8,9-dihydroxy-14-methoxy-3-methyl-3,4,9,10-tetrahydro-1*H* benzo[*c*][1]oxacyclotetradecine-1,7,16(8*H*,13*H*)-trione (**11**)[24]

Selectfluor® (180 mg, 0.50 mmol) was added to a solution of (5*Z*)-7-oxozeaenol (30 mg, 0.083 mmol) in CH_3CN (3 mL) and the mixture stirred for 3 h at room temperature. The solvent was evaporated and the residue was diluted with ethyl acetate (5 mL) and washed with water (5 mL). The organic layer was dried using anhydrous sodium sulfate, filtered and the solvent evaporated. The residue was purified by preparative HPLC using a Phenomenex Gemini-NX column C18 (250 × 21.20 mm, 110 A, 5 µm spherical particle size). The column was perfused at a flow rate of 21.24 mL/min with 60% (water, 0.1% TFA), and 40% of (MeOH) over 40 min. The compound eluted at ~30 min. UPLC was employed to evaluate the purity using a gradient solvent system that initiated with 20:80 CH_3CN−H_2O to 100% CH_3CN over 4.5 min (>97% pure based on the ELSD detector; Fig. S2, SI). Yield (27 mg, 14%). ^{1}H NMR (500 MHz, $CDCl_3$) δ 6.63 (dt, J_d = 11.5 Hz, J_t = 4.0 Hz, 1H; 5-H), 6.38–6.27 (m, 1H; 11-H), 6.31 (d, J = 11.5 Hz, 1H; 6-H), 6.07 (d, J = 15.5 Hz, 1H; 12-H), 5.58 (t, J = 2.3 Hz, 1H; 16-H), 5.43 (ddq, J_q = 6.3 Hz, J_d = 1.2, 10.3 Hz, 1H; 3-H), 4.47 (bs, 1H; 8-H), 4.13–4.11 (m, 1H; 9-H), 3.85 (s, 3H; 20-H), 3.86–3.85 (m, 1H; 3-H), 2.57 (ddd, J = 6.9, 8.0, 15.5 Hz, 1H; 10-H), 2.46 (d, 16.0 Hz, 1H; 4-H), 2.37 (dd, J = 15.5, 5.2 Hz, 1H; 10-H), 1.41 (d, J = 6.3 Hz, 3H; 19-H). ^{13}C NMR (125 MHz, $CDCl_3$) δ 198.3, 181.4, 164.2, 163.1 (t, J = 24.0 Hz, 1C; 15-C), 150.4, 140.2, 138.3 (t, J = 25.0 Hz, 1C; 13-C), 130.3 (t, J = 5.8 Hz, 1C; 18-C), 123.1, 122.7, 108.9 (t, J = 241.5 Hz, 1C; 14-C), 102.3 (t, J = 3.8 Hz, 1C; 16-C), 80.7, 73.8, 72.6, 57.0, 38.1, 37.2, 21.4. HRMS (ESI, *m*/*z*): Calculated for $C_{19}H_{21}F_2O_7$ $[M+H]^+$ 399.1250; found 399.1242 (2.0 ppm).

4.2.4. (3*S*,5*Z*,8*S*,9*S*,11*E*)-15-Bromo-8,9,16-trihydroxy-14-methoxy-3-methyl-3,4,9,10-tetrahydro-1*H*-benzo[*c*][1]oxacyclotetradecine-1,7(8*H*)-dione (**12**)[26]

N-Bromosuccinimide (7.4 mg, 0.041 mmol) was added to a solution of (5*Z*)-7-oxozeaenol (15 mg, 0.041 mmol) in $CHCl_3$ (1 mL) and the mixture stirred for 4 h at room temperature. $CHCl_3$ (4 mL) was added to the mixture and it was washed with water (5 mL). The organic layer was dried using anhydrous sodium sulfate, filtered and the solvent evaporated. The solvent was evaporated and the residue was purified by preparative HPLC using a Phenomenex Gemini-NX column C18 (250 × 21.20 mm, 110 A, 5 µm spherical particle size). The column was perfused at a flow rate of 21.24 mL/min with a linear gradient from 40% (CH_3CN–H_2O) to 50% over 15 min. The compound eluted at 18.5 min. UPLC was used to evaluate the purity using a gradient solvent system that initiated with 20:80 CH_3CN−H_2O to 100% CH_3CN over 4.5 min (>97% pure; Fig. S1, SI). Yield (1.76 mg, 14%). ^{1}H NMR (500 MHz, $CDCl_3$) δ 12.79 (s, 1H; 17-OH), 6.88 (d, J = 15.3 Hz, 1H; 12-H), 6.42 (s, 1H; 14-H), 6.34 (dd, J = 11.5, 3 Hz, 1H; 6-H), 6.22 (ddd, J = 2.3, 3.0, 11.5 Hz, 1H; 5-H), 6.03 (ddd, J = 15.3, 10.7, 4.6 Hz, 1H; 11-H), 5.26 (ddq, J_d = 1.5, 8.5 Hz, J_q = 6.1 Hz, 1H; 3-H), 4.53 (dd, J = 2.3, 5.4 Hz, 1H; 8-H), 4.00 (bs, 1H; 9-H), 3.95 (s, 3H; 20-H), 3.57 (ddd, J = 5.4, 10.7, 11.5 Hz, 1H; 4-H), 2.53 (dd, J = 2.3, 17.6 Hz, 1H; 4-H), 2.23–2.11 (m, 2H; 10-H), 1.48 (d, J = 6.1 Hz, 3H; 19-H). ^{13}C NMR (100 MHz, $CDCl_3$) δ 199.0, 171.1, 161.4, 160.4, 147.6, 142.3, 132.9, 131.1, 125.3, 104.8, 103.7, 99.1, 80.9, 74.6, 73.6, 56.5, 37.5, 37.1, 20.8. HRMS (ESI, *m*/*z*): Calculated for $C_{19}H_{22}{}^{79}BrO_7$ $[M+H]^+$ 441.0543; found 441.0546 (0.6 ppm), Calculated for $C_{19}H_{22}{}^{81}BrO_7$ $[M+H]^+$ 443.0523; found 443.0521 (0.4 ppm).

4.2.5. (3*S*,5*Z*,8*S*,9S,11*E*)-13-Bromo-8,9,16-trihydroxy-14-methoxy-3-methyl-3,4,9,10-tetrahydro-1*H*-benzo[*c*][1]oxacyclotetradecine-1,7(8*H*)-dione[26] (**13**)

Same as procedure described for synthesis of compound **12**. Compound **13** eluted at 14.5 min. UPLC was used to evaluate the purity using a gradient solvent system that initiated with 20:80 $CH_3CN{-}H_2O$ to 100% CH_3CN over 4.5 min (>97% pure; Fig. S1, SI). Yield (6.4 mg, 52%). ^{1}H NMR (500 MHz, $CDCl_3$) δ 12.12 (s, 1H; 17-OH), 6.43 (s, 1H; 16-H), 6.39 (dd, J = 15.3, 2 Hz, 1H; 12-H), 6.31 (dd, J = 11.5, 2.9 Hz, 1H; 6-H), 6.18 (dt, J_d = 2.9 Hz, J_t = 10.9 Hz, 1H; 5-H), 5.72 (ddd, J = 3.4, 10.3, 16.0 Hz, 1H; 11-H), 5.40 (ddq, J_d = 1.7, 8.5 Hz, J_q = 6.1 Hz, 1H; 3-H), 4.55 (bs, 1H; 8-H), 3.95 (bs, 1H; 9-H), 3.89 (s, 3H; 20-H), 3.74 (d, J = 4.0 Hz, 1H; 8-OH), 3.35 (ddd, J = 10.9, 11.5, 17.2 Hz, 1H; 4-H), 2.51 (dd, J = 2.3, 17.2 Hz, 1H; 4-H), 2.33 (ddd, J = 2.3, 4.3, 16.6 Hz, 1H; 10-H), 2.10 (ddd, J = 2.9, 10.3, 16.6 Hz, 1H; 10-H), 1.46 (d, J = 6.1 Hz, 3H; 19-H). ^{13}C NMR (125 MHz, $CDCl_3$) δ 199.4, 170.9, 164.4, 161.1, 146.6, 142.2, 133.9, 129.6, 125.6, 105.8, 105.4, 99.5, 81.0, 73.8, 73.1, 56.7, 37.0, 36.8, 21.0. HRMS (ESI, *m*/*z*): Calculated for $C_{19}H_{22}{}^{79}BrO_7[M+H]^+$ 441.0543; found 441.0546 (0.6 ppm), Calculated for $C_{19}H_{22}{}^{81}BrO_7$ $[M+H]^+$443.0523; found 443.0522 (0.2 ppm).

4.2.6. (3*S*,5*Z*,8*S*,9*S*,11*E*)-13,15-Dibromo-8,9,16-trihydroxy-14methoxy-3-methyl-3,4,9,10-tetrahydro-1*H*-benzo[*c*][1]oxacyclotetradecine-1,7(8*H*)-dione (**14**)[26]

Same as procedure described for synthesis of compound **12**. Compound **14** eluted at 21 min. UPLC was used to evaluate the purity using a gradient solvent system that initiated with 20:80 $CH_3CN{-}H_2O$ to 100% CH_3CN over 4.5 min (>97% pure; Fig. S1, SI). Yield (1.4 mg, 10%). ^{1}H NMR (500 MHz, $CDCl_3$) δ 12.46 (s, 1H; 17-OH), 6.37 (d, J = 16.0 Hz, 1H; 12-H), 6.32 (dd, J = 11.5, 2.9 Hz, 1H; 6-H), 6.20 (ddd, J = 2.9, 10.9, 11.5 Hz, 1H; 5-H), 5.72 (ddd, J = 3.4, 10.3, 16.0 Hz, 1H; 11-H), 5.47 (ddq, J_q = 6.3, J_d = 1.7, 11.5 Hz, 1H; 3-H), 4.55 (dd, J = 5.2, 2.3 Hz, 1H; 8-H), 3.95 (bs, 1H; 9-H), 3.90 (s, 3H; 20-H), 3.72 (d, J = 5.2 Hz, 1H; 8-OH), 3.40 (ddd, J = 10.9, 11.5, 17.2 Hz, 1H; 4-H), 2.53 (ddd, J = 2.3, 2.9, 17.2 Hz, 1H; 4-H), 2.36–2.31 (m, 2H; 10-H, 9-OH), 2.13 (ddd, J = 2.3, 10.3, 16.6 Hz, 1H; 10-H), 1.39 (d, J = 6.3 Hz, 3H; 19-H). ^{13}C NMR (100 MHz, $CDCl_3$) δ 199.2, 170.5, 160.0, 159.6, 146.4, 141.3, 134.6, 129.1, 125.1, 104.7, 103.6, 99.0, 80.9, 74.8, 73.0, 60.6, 37.0, 36.8, 20.8. HRMS (ESI, *m*/*z*): Calculated for $C_{19}H_{21}{}^{79}Br_2O_7$ $[M+H]^+$ 518.9648; found 518.9633 (3.0 ppm), Calculated for $C_{19}H_{21}{}^{79}Br^{81}BrO_7$ $[M+H]^+$ 520.9628; found 520.9613 (2.9 ppm), Calculated for $C_{19}H_{21}{}^{81}Br_2O_7$ $[M+H]^+$ 522.9608; found 522.9593 (2.8 ppm).

4.2.7. (12*S*,13*S*,8*S*,*E*)-13,53-Dihydroxy-55-methoxy-8-methyl13,14,15,16-tetrahydro-12*H*-7-oxa-1(2,6)-pyrana-5(1,2)benzenacyclononaphan-3-ene-14,6-dione (**15**)[28]

p-Toluenesulfonic acid (0.5 mg, 0.003 mmol) was added to a solution of (5*Z*)-7-oxozeaenol (5.0 mg, 0.014 mmol) in CH_2Cl_2 (2 mL) and the mixture stirred overnight at room temperature. The reaction mixture was quenched with 10% aqueous $NaHCO_3$ (2 mL), the organic layer dried using anhydrous sodium sulfate and the solvent evaporated. The residue was purified by preparative HPLC using a Phenomenex Gemini-NX column C18 (250 × 21.20 mm, 110 A, 5 µm spherical particle size). The column was perfused at a flow rate of 21.24 mL/min with solvent A (water, 0.1% TFA), and a linear gradient from 40% to 50% of solvent B (CH_3CN) over 30 min. The compound eluted at 28.5 min. UPLC was used to evaluate the purity using a gradient solvent system that initiated with 20:80 $CH_3CN{-}H_2O$ to 100% CH_3CN over 4.5 min (>97% pure; Fig. S1, SI). Yield (1.8 mg, 35%). ^{1}H NMR (400 MHz, $CDCl_3$) δ 11.19 (s, 1H; 17-OH), 7.13

(d, J = 16.0 Hz, 1H; 12-H), 6.36 (d, J = 2.8 Hz, 1H; 16-H), 6.33 (d, 2.8 Hz, 1H; 14-H), 5.83 (ddd, J = 6.4, 6.9, 16.0 Hz, 1H; 11-H), 5.20–5.12 (m, 1H; 3-H), 4.68–4.63 (m, 1H; 5-H), 4.11 (dd, J = 9.6, 4.1 Hz, 1H; 8-H), 3.85 (ddd, J = 2.8, 8.2, 10.1 Hz, 1H; 9-H), 3.80 (s, 3H; 20-H), 3.55 (d, J = 4.1 Hz, 1H; 8-OH), 2.89 (dd, J = 15.1, 6.9 Hz, 1H; 6-H), 2.72 (dd, J = 7.0, 14.5 Hz, 1H; 10-H), 2.48 (dd, J = 15.1, 3.7 Hz, 1H; 6-H), 2.44–2.38 (m, 1H; 10-H), 2.21 (ddd, J = 4.1, 6.6, 8.2 Hz, 1H; 4-H), 1.56–1.54 (m, 1H; 4-H), 1.41 (d, J = 6.0 Hz, 3H; 19-H). ^{13}C NMR (100 MHz, $CDCl_3$) δ207.6, 171.2, 164.3, 164.1, 143.7, 135.7, 125.7, 107.5, 105.1, 99.8, 77.7, 76.2, 73.6, 72.4, 55.5, 46.2, 37.2, 33.3, 21.7. HRMS (ESI, m/z): Calculated for $C_{19}H_{23}O_7$ $[M+H]^+$ 363.1438; found 363.1433 (1.5 ppm).

4.2.8. (3a*S*,5*Z*,8*S*,15*E*,17a*S*)-11-Hydroxy-13-methoxy-2,2,8-trimethyl-7,8,17,17a-tetrahydro-4*H*-benzo[*c*][1,3]dioxolo[4,5-*h*][1]oxacyclotetradecine-4,10(3a*H*)-dione (**16**)[10]

p-Toluenesulfonic acid (2.0 mg, 0.012 mmol, 9 mol %) was added to a suspension of (5*Z*)-7-oxozeaenol (50.0 mg, 0.138 mmol) in dimethoxypropane (20 mL) and the mixture stirred for an hour at room temperature. Dimethoxypropane was evaporated, the residue dissolved in $CHCl_3$ (20 mL), and the reaction quenched with 10% aqueous $NaHCO_3$(10 mL). The organic layer was dried over anhydrous magnesium sulfate and the solvent evaporated. The residue was purified by preparative HPLC using a Phenomenex Gemini-NX C18 column (250 × 21.20 mm, 110 A, 5 µm spherical particle size). The column was perfused at a flow rate of 21.24 mL/min with (water, 0.1% TFA), and a linear gradient from 60% to 70% of (CH_3CN) over 15 min. The compound eluted at 16.5 min. UPLC was used to establish purity using a gradient solvent system that initiated with 20:80 CH_3CN/H_2O to 100% CH_3CN over 4.5 min (>97% pure; Fig. S1, SI). Not all signals were observed in the ^{1}H and ^{13}C NMR spectra due to the equilibration of distinct conformers. Definitive structural assignment was determined by the hydrolysis of the acetonide to regenerate (5*Z*)-7-oxozeaenol where 16 (2 mg, 0.005 mmol) was dissolved in MeOH and 1 drop of HCl (1 M) was added. The formation of 1 was monitored using ^{1}H NMR. Yield (23.6 mg, 43%). ^{1}H NMR (500 MHz, $CDCl_3$) δ 12.07 (s, 1H; 17-OH), 6.93 (d, J = 15.1 Hz, 1H; 12-H), 6.36 (s, 2H; 14-H and 16-H), 5.73–5.67 (m, 1H; 11-H), 5.37 (bs, 1H; 3-H), 4.58–4.54 (m, 2H; 8-H and 9-H), 3.79 (s, 3H; 20-H), 2.67–2.58 (m, 2H; 3-H), 1.57 (s, 3H; 21-H), 1.47 (d, J = 6.4 Hz, 3H; 19-H). 1.38 (s, 3H; 22-H). ^{13}C NMR (100 MHz, $CDCl_3$) δ 196.5 (m, 7-C=O), 171.1, 165.6, 163.9, 146.3 (m; 5-C), 142.6, 133.6, 127.1 (m; 6-C), 126.6, 110.0, 108.9, 103.6, 100.1, 81.7 (m; 8-C), 77.2, 72.9 (m; 3-C), 55.4, 35.8, 27.0, 25.2 (m; $(CH_3)_2$), 19.9 (m; 19-C). HRMS: (ESI, m/z): Calculated for $C_{22}H_{27}O_7$ $[M+H]^+$ 403.1751; found 403.1749 (0.6 ppm).

4.3. Computational calculations and covalent docking

All calculations were carried out using SPARTAN'08 for Linux. Initial conformational analyses were carried out on each ligand using a Monte-Carlo molecular mechanics conformational search using the RM1/semi-empirical force field at the ground state. All resulting conformations with E_{rel} less than 10 kcal/mol, relative to the lowest-energy conformation, were then modeled using Hartree–Fock with the 6-31G* basis set in the gas phase. The resulting global minimum was exported to Maestro as mol.2 file and subjected to covalent docking.

Prior to covalent docking, the crystal structure (PDB ID: 4GS6) was prepared using protein preparation wizard, implemented in Maestro, where hydrogens were added to all atoms and bond

orders were assigned. The covalent linkage between the co-crystalized (5*Z*)-7-oxozeaenol TAK1 enzyme was broken, the ligand deleted and the bare enzyme used as the binding protein for docking. Covalent docking, implemented in Glide, was used to evaluate the relative binding affinities of the various ligands tested. The reaction type chosen was Michael addition where amino acid Cysteine 174 was identified as the reactive reside. The grid box was determined as the centroid of residues Cysteine 174, valine 42 and alanine 46. Cysteine 174 was not chosen as the sole determinant of the grid box because it is impeded at the back of the binding pocket thus will not result in spanning the biding site efficiently. Many residue combinations were screened and the aforementioned collection was representative of a box holding all atoms of the co-crystalized (5*Z*)-7-oxozeaenol in the original crystal structure.

The initial covalent docking output with the highest score for each docked ligand was minimized using prime, implemented in Maestro. All atoms including those of the enzyme and the ligand were minimized using VSGB solvation model. The number of iterations implemented for the automatic method of minimization was 8 and steps per iterations were 200. The covalent linkage between the docked ligand and the enzyme was broken again and the minimized ligand was covalently docked in the minimized enzyme.

4.4. TAK1 inhibition assays

The assay was performed at BSP Bioscience Inc. (5*Z*)-7-oxozeaenol was used as a positive control. Detailed experimental procedures are provided in the Supporting information.

Acknowledgments

This research was supported in part by the National Cancer Institute/National Institutes of Health (program project grant P01 CA125066). The authors thank Dr. Franklin J. Moy (UNCG) for assisting with analysis of NMR data and Dr. Brandie M. Ehrmann (UNCG) for acquisition of the high resolution mass spectrometry data at the Triad Mass Spectrometry Laboratory at the University of North Carolina at Greensboro.

Supplementary data

Supplementary data may be found at the end of this formatted document.

References and notes

1. Yamaguchi, K.; Shirakabe, K.; Shibuya, H.; Irie, K.; Oishi, I.; Ueno, N.; Taniguchi, T.; Nishida, E.; Matsumoto, K. Science 2008, 1995, 270.

2. Schuman, J.; Chen, Y.; Podd, A.; Yu, M.; Liu, H.-H.; Wen, R.; Chen, Z. J.; Wang, D. Blood 2009, 113, 4566.

3. Ninomiya-Tsuji, J.; Kishimoto, K.; Hiyama, A.; Inoue, J.; Cao, Z.; Matsumoto, K. Nature 1999, 398, 252.

4. Johnson, G. L.; Dohlman, H. G.; Graves, L. M. Curr. Opin. Chem. Biol. 2005, 9, 325.

5. Singh, A.; Sweeney, M. F.; Yu, M.; Burger, A.; Greninger, P.; Benes, C.; Haber, D. A.; Settleman, J. Cell 2012, 148, 639.

6. (a) Dakas, P.-Y.; Barluenga, S.; Totzke, F.; Zirrgiebel, U.; Winssinger, N. Angew. Chem., Int. Ed. 2007, 46, 6899; (b) Jogireddy, R.; Dakas, P.-Y.; Valot, G.; Barluenga, S.; Winssinger, N. Chem. Eur. J. 2009, 15, 11498; (c) Du, H.; Matsushima, T.; Spyvee, M.; Goto, M.; Shirota, H.; Gusovsky, F.; Chiba, K.; Kotake, M.; Yoneda, N.; Eguchi, Y.; DiPietro, L.; Harmange, J. C.; Gilbert, S.; Li, X. Y.; Davis, H.; Jiang, Y.; Zhang, Z.; Pelletier, R.; Wong, N.; Sakurai, H.; Yang, H.; Ito-Igarashi, H.; Kimura, A.; Kuboi, Y.; Mizui, Y.; Tanaka, I.; Ikemori-Kawada, M.; Kawakami, Y.; Inoue, A.; Kawai, T.; Kishi, Y.; Wang, Y. Bioorg. Med. Chem. Lett. 2009, 19, 6196; (d) Jogireddy, R.; Barluenga, S.; Winssinger, N. ChemMedChem 2010, 5, 670; (e) Barluenga, S.; Jogireddy, R.; Koripelly, G. K.; Winssinger, N. ChemBioChem 2010, 11, 1692.

7. Meng, F.; Li, Y.; Tian, X.; Fu, L.; Yin, Y.; Sui, C.; Ma, P.; Jiang, Y. Biochem. Biophys. Res. Commun. 2014, 453, 106.

8. Wang, Y.; Tu, Q.; Yan, W.; Xiao, D.; Zeng, Z.; Ouyang, Y.; Huang, L.; Cai, J.; Zeng, X.; Chen, Y. J.; Liu, A. Biochem. Biophys. Res. Commun. 2014, 456, 373.

9. Melisi, D.; Xia, Q.; Paradiso, G.; Ling, J.; Moccia, T.; Carbone, C.; Budillon, A.; Abbruzzese, J. L.; Chiao, P. J. J. Natl. Cancer Inst. 2011, 103, 1190.

10. Ellestad, G. A.; Lovell, F. M.; Perkinson, N. A.; Hargreaves, R. T.; McGahren, W. J. J. Org. Chem. 1978, 43, 2339.

11. Schirmer, A.; Kennedy, J.; Murli, S.; Reid, R.; Santi, D. V. Proc. Natl. Acad. Sci. U.S.A. 2006, 103, 4234.

12. Ninomiya-Tsuji, J.; Kajino, T.; Ono, K.; Ohtomo, T.; Matsumoto, M.; Shiina, M.; Mihara, M.; Tsuchiya, M.; Matsumoto, K. J. Biol. Chem. 2003, 278, 18485.

13. Zhang, J.; Yang, P. L.; Gray, N. S. Nat. Rev. Cancer 2009, 9, 28.

14. Wu, J.; Powell, F.; Larsen, N. A.; Lai, Z.; Byth, K. F.; Read, J.; Gu, R. F.; Roth, M.; Toader, D.; Saeh, J. C.; Chen, H. ACS Chem. Biol. 2013, 8, 643.

15. Singh, J.; Petter, R. C.; Baillie, T. A.; Whitty, A. Nat. Rev. Drug Disc. 2011, 10, 307.

16. Kilty, I.; Green, M. P.; Bell, A. S.; Brown, D. G.; Dodd, P. G.; Hewson, C.; Hughes, S. J.; Phillips, C.; Ryckmans, T.; Smith, R. T.; van Hoorn, W. P.; Cohen, P.; Jones, L. H. Chem. Biol. Drug Des. 2013, 82, 500.

17. Ayers, S.; Graf, T. N.; Adcock, A. F.; Kroll, D. J.; Matthew, S.; Carcache de Blanco, E. J.; Shen, Q.; Swanson, S. M.; Wani, M. C.; Pearce, C. J.; Oberlies, N. H. J. Nat. Prod. 2011, 74, 1126.

18. El-Elimat, T.; Raja, H. A.; Day, C. S.; Chen, W. L.; Swanson, S. M.; Oberlies, N. H. J. Nat. Prod. 2014, 77, 2088.

19. Wu, H.; Thatcher, L. N.; Bernard, D.; Parrish, D. A.; Deschamps, J. R.; Rice, K. C.; MacKerell, A. D.; Coop, A. Org. Lett. 2005, 7, 2531.

20. Pinkerton, A. B.; Vernier, J. -M.; Cube, R. V.; Hutchinson, J. H.; Huang, D.; Bonnefous, C.; Govak, S. P.; Kamenecka, T. WO 2005US26425 20050726, 2006.

21. Dean, M. A.; Hitchcock, S. R. Tetrahedron: Asymmetry 2010, 21, 2471.

22. Zea-Ponce, Y.; Mavel, S.; Assaad, T.; Kruse, S. E.; Parsons, S. M.; Emond, P.; Chalon, S.; Giboureau, N.; Kassiou, M.; Guilloteau, D. Bioorg. Med. Chem. 2005, 13, 745.

23. Wang, J.; Sánchez-Roselló, M.; Aceña, J. L.; del Pozo, C.; Sorochinsky, A. E.; Fustero, S.; Soloshonok, V. A.; Liu, H. Chem. Rev. 2013, 114, 2432.

24. Woodhead, A. J.; Angove, H.; Carr, M. G.; Chessari, G.; Congreve, M.; Coyle, J. E.; Cosme, J.; Graham, B.; Day, P. J.; Downham, R.; Fazal, L.; Feltell, R.; Figueroa, E.; Frederickson, M.; Lewis, J.; McMenamin, R.; Murray, C. W.; O'Brien, M. A.; Parra, L.; Patel, S.; Phillips, T.; Rees, D. C.; Rich, S.; Smith, D.-M.; Trewartha, G.; Vinkovic, M.; Williams, B.; Woolford, A. J. A. J. Med. Chem. 2010, 53, 5956.

25. Langlois, B. R.; Laurent, E.; Roidot, N. Tetrahedron Lett. 1991, 32, 7525.

26. Dijkstra, P. J.; Den Hertog, H. J.; Van Steen, B. J.; Zijlstra, S.; Skowronska- Ptasinska, M.; Reinhoudt, D. N.; Van Eerden, J.; Harkema, S. J. Org. Chem. 1987, 52, 2433.

27. Xu, J.; Chen, A.; Go, M.-L.; Nacro, K.; Liu, B.; Chai, C. L. L. ACS Med. Chem. Lett. 2011, 2, 662.

28. Schmidt, B.; Staude, L.; Kelling, A.; Schilde, U. Eur. J. Org. Chem. 2011, 2011, 1721.

29. Zhu, K.; Borrelli, K. W.; Greenwood, J. R.; Day, T.; Abel, R.; Farid, R. S.; Harder, E. J. Chem. Inf. Model 2014, 54, 1932.

Supporting Information

Isolation, semisynthesis, covalent docking and transforming growth factor beta-activated kinase 1 (TAK1)-inhibitory activities of (5Z)-7-oxozeaenol analogues

Lara, Fakhouri, Tamam, El-Elimat, Dow P. Hurst, Patricia, H. Reggio, Cedric J. Pearce, Nicholas H. Oberlies and Mitchell P. Croatt

Table of Contents for Supporting Information

TAK1 Inhibition Assay Procedure

The assay was performed using Kinase–Glo Plus luminescence kinase assay kit (Promega). It measures kinase activity by quantifying the amount of ATP remaining in solution following a kinase reaction. The luminescent signal from the assay is correlated with the amount of ATP present and is inversely correlated with the amount of kinase activity. Compounds were diluted in 10% DMSO and 5 µL of the dilution was added to a 50 µL reaction so that the final concentration of DMSO is 1% in all of reactions. The compounds were preincubated with the enzyme in a reaction mixture for 10 min at room temperature. The enzymatic reactions were initiated by adding ATP (20 µM at final) and conducted for 40 min at 30 °C. The 50 µL reaction mixture contained 40 mM Tris, pH 7.4, 10 mM $MgCl_2$, 0.1 mg/mL BSA, 1 mM DTT, 0.2 mg/mL MBP substrate, 20 µM ATP and Tak1–TAB1. After the enzymatic reaction, 50 µL of Kinase–Glo Plus Luminescence kinase assay solution (Promega) was added to each reaction, and the plate was incubated for 20 min at room temperature. Luminescence signal was measured using a BioTek Synergy 2 microplate reader. Tak1–TAB1 activity assays were performed in duplicate at each concentration. The luminescence data were analyzed using the computer software, Graphpad Prism. The difference between luminescence intensities in the absence of Tak1–TAB1 (Lut) and in the presence of Tak1–TAB1 (Luc) was defined as 100% activity (Lut – Luc). Using luminescence signal (Lu) in the presence of the compound, % activity was calculated as: % activity = [(Lut – Lu)/(Lut – Luc)]×100%, where Lu= the luminescence intensity in the presence of the compound. The values of % activity versus a series of compound concentrations were then plotted using non–linear regression analysis of Sigmoidal dose–response curve generated with the equation Y=B+(T–B)/1+10((LogEC_{50}–X)×Hill Slope), where Y = percent activity, B = minimum percent activity, T = maximum percent activity, X = logarithm of compound and Hill Slope = slope factor or Hill coefficient. The IC_{50} values were determined by the concentration causing a half–maximal percent activity.

UPLC Chromatograms of Compounds 1, 10-16

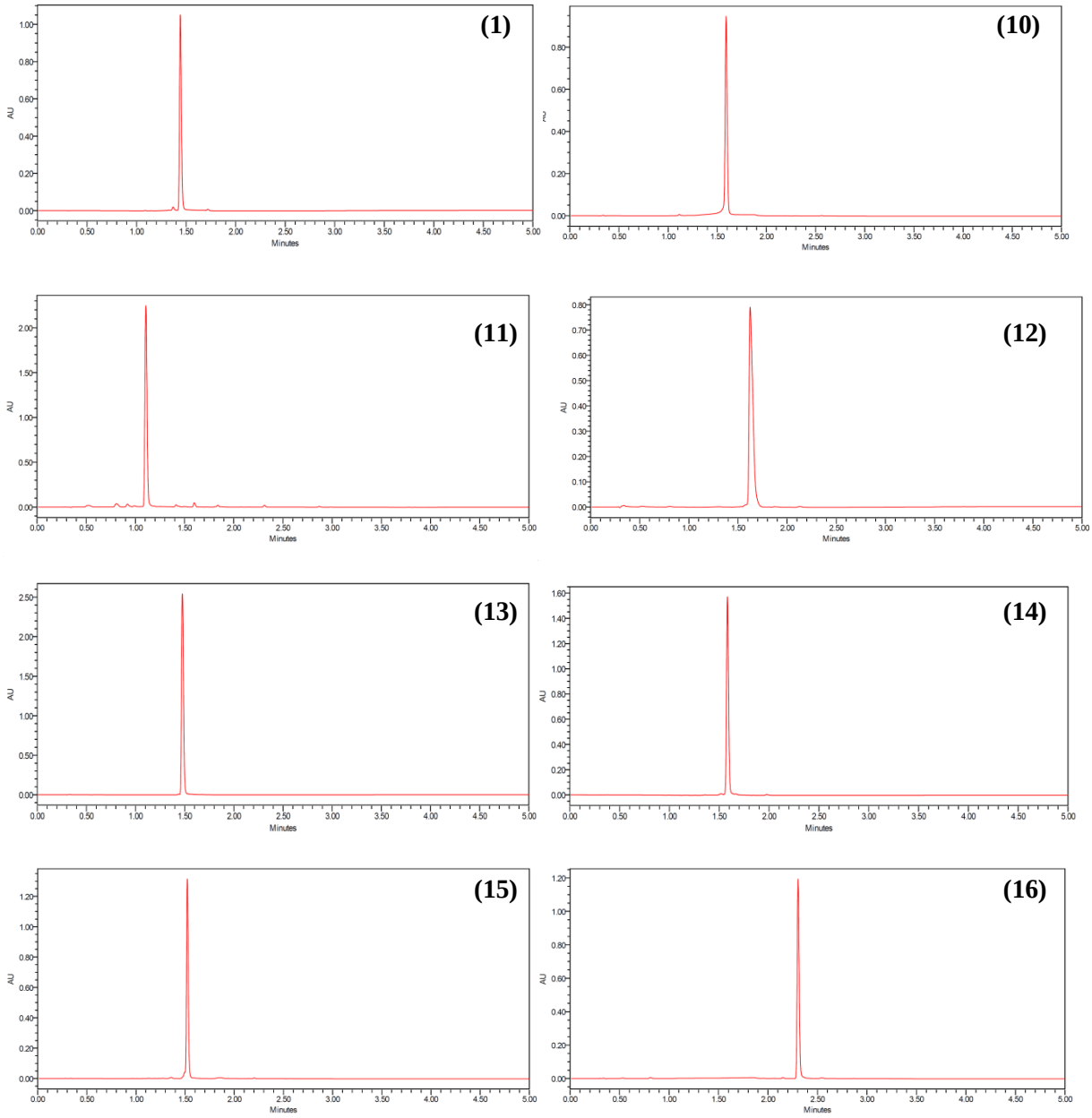

Figure S1. UPLC chromatograms of compounds **1**, **10-16** (λ 254 nm), demonstrating >96% purity. All data were acquired via an Acquity UPLC system with a Phenomenex Kinetex C18 (1.3 µm; 50 × 2.1 mm) column and a CH_3CN/H_2O gradient that increased linearly from 20 to 100% CH_3CN over 1.2 min.

NMR Data for Compounds 9-16

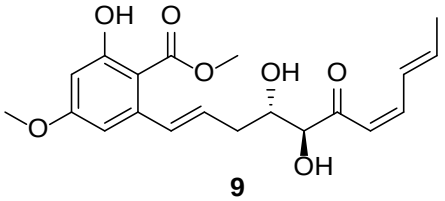

9

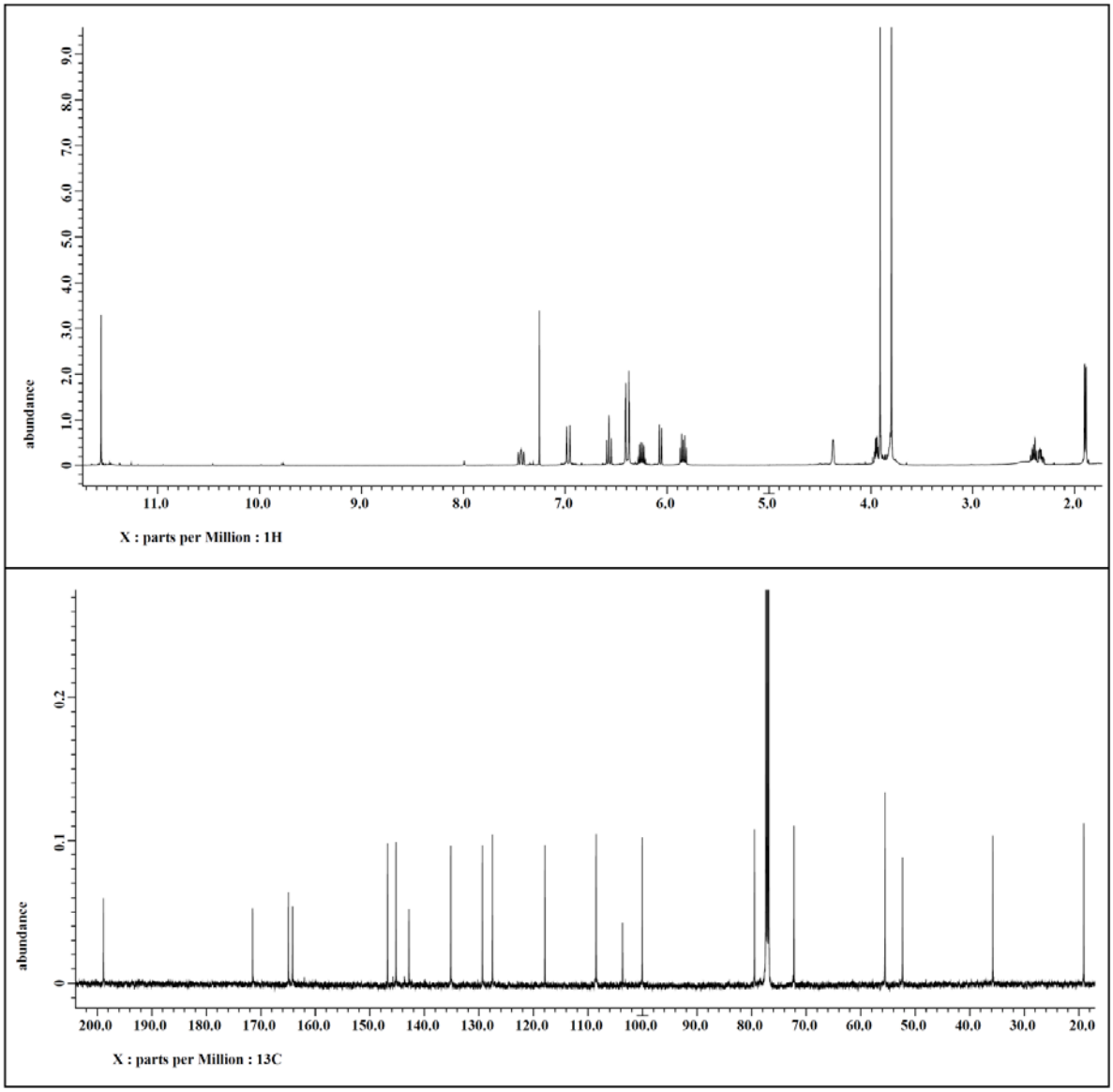

Figure S2. ^{1}H and ^{13}C NMR spectra of compound **9** [500 MHz for ^{1}H and 125 MHz for ^{13}C, $CDCl_3$]

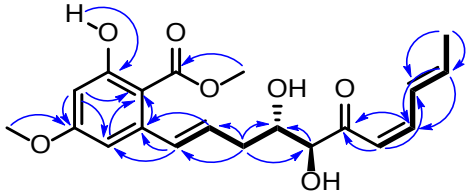

Figure S3. Major COSY (—) and HMBC (blue arrows) correlations of compound **9**

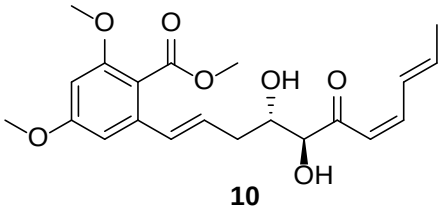

10

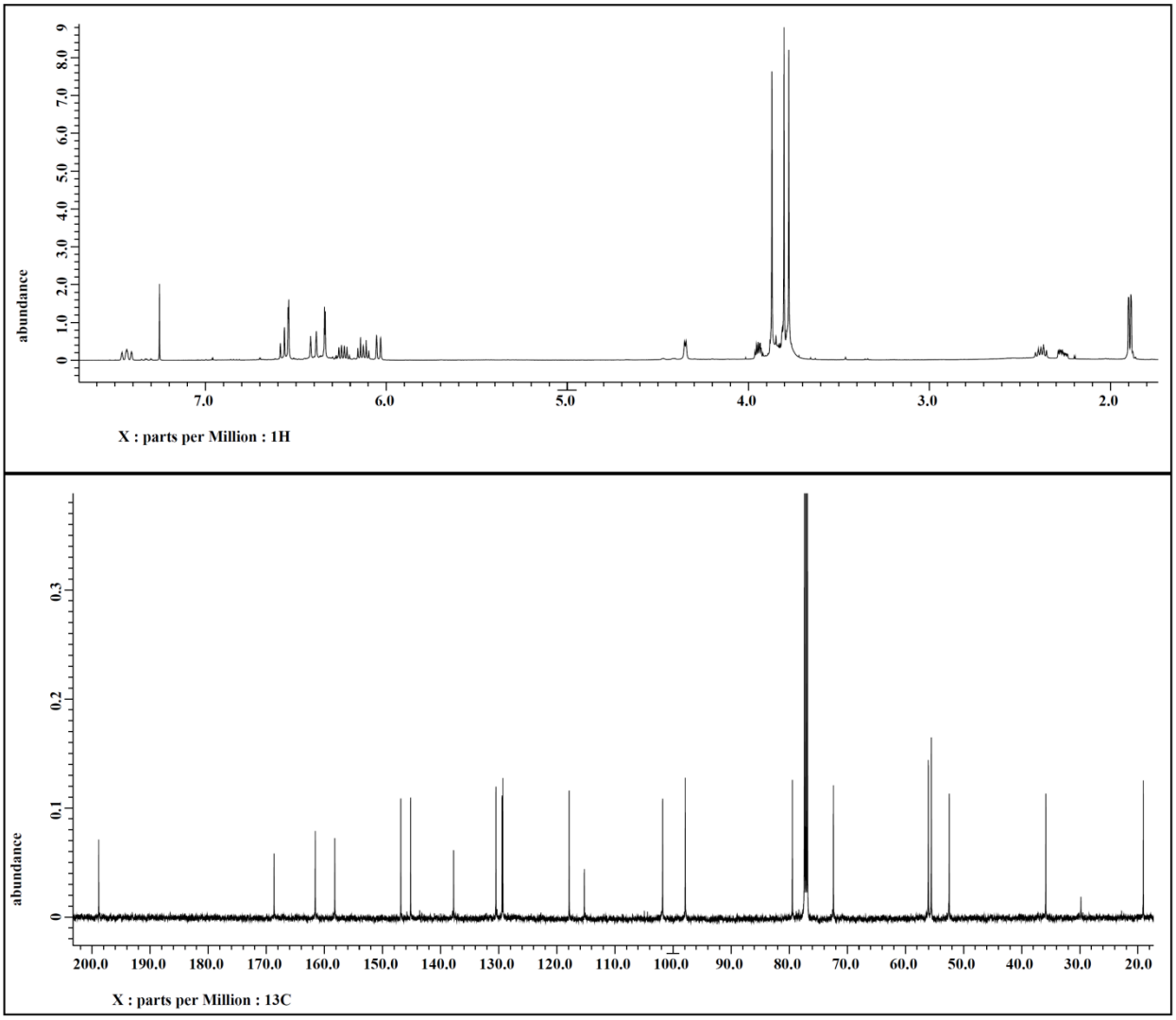

Figure S4. ^{1}H and ^{13}C NMR spectra of compound **10** [500 MHz for ^{1}H and 125 MHz for ^{13}C, $CDCl_3$]

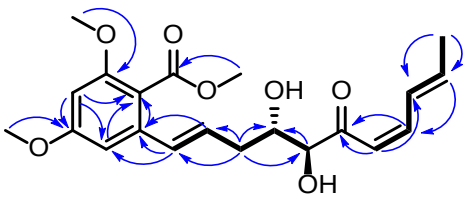

Figure S5. Major COSY (—) and HMBC (blue arrows) correlations of compound **10**

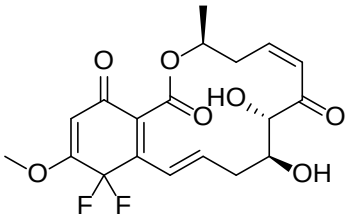

11

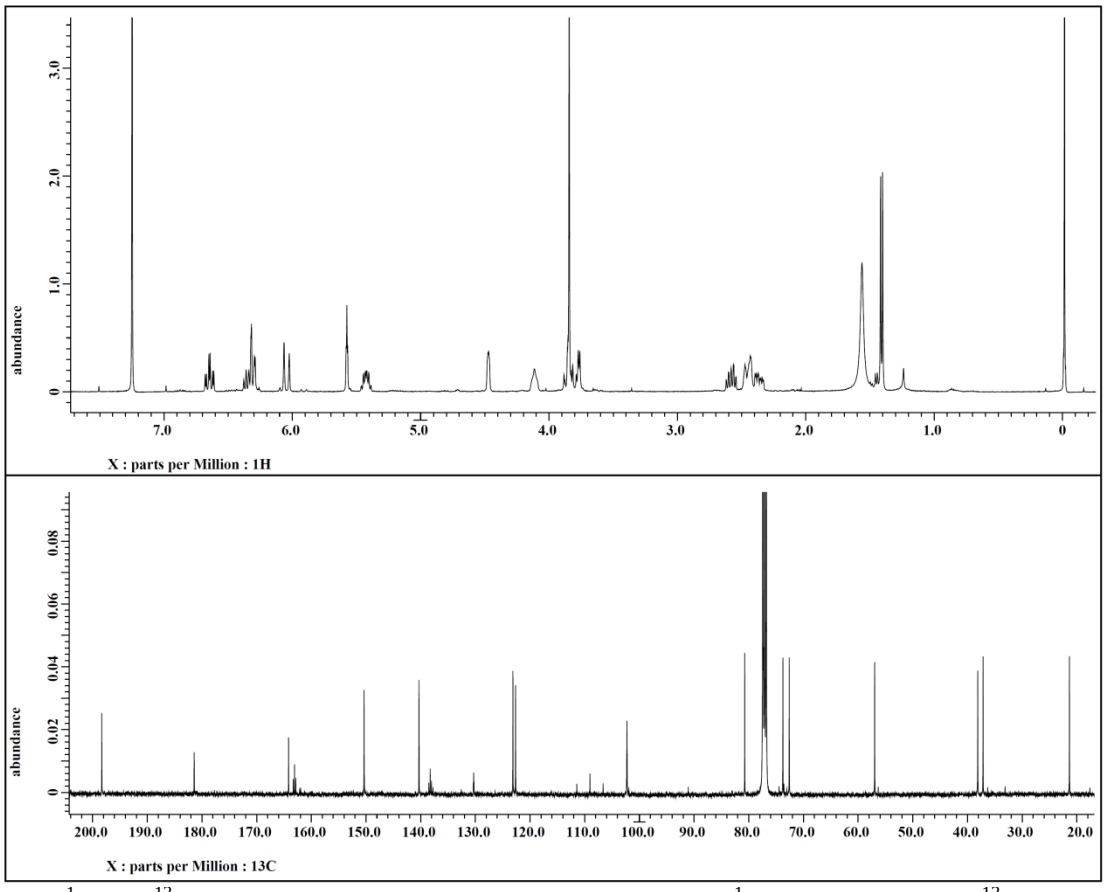

Figure S6. ^{1}H and ^{13}C NMR spectra of compound **11** [500 MHz for ^{1}H and 125 MHz for ^{13}C, $CDCl_3$]

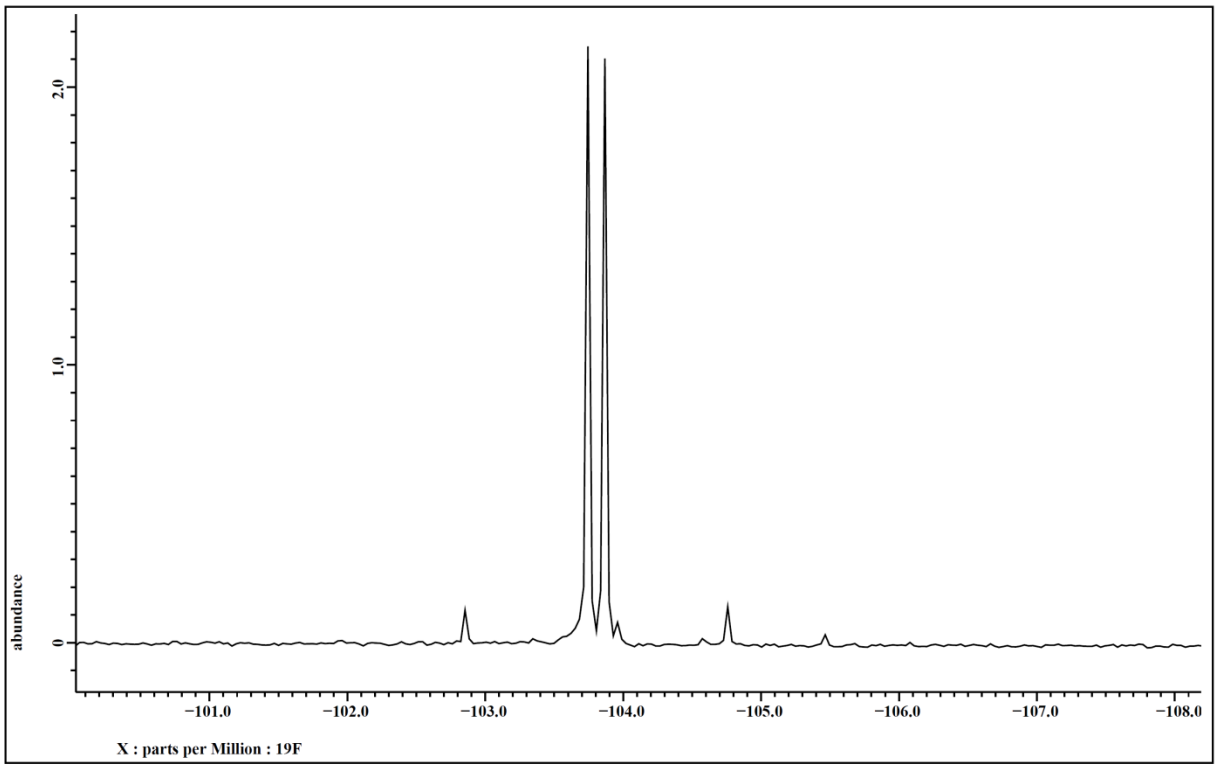

Figure S7. ^{19}F NMR spectra of compound **11** [375 MHz, $CDCl_3$]

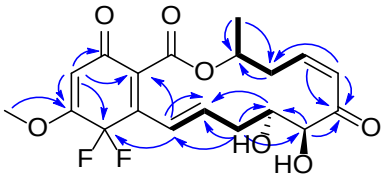

Figure S8. Major COSY (—) and HMBC (blue arrows) correlations of compound **11**

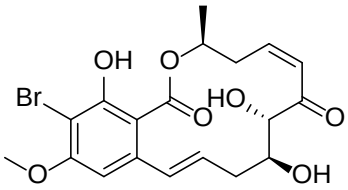

12

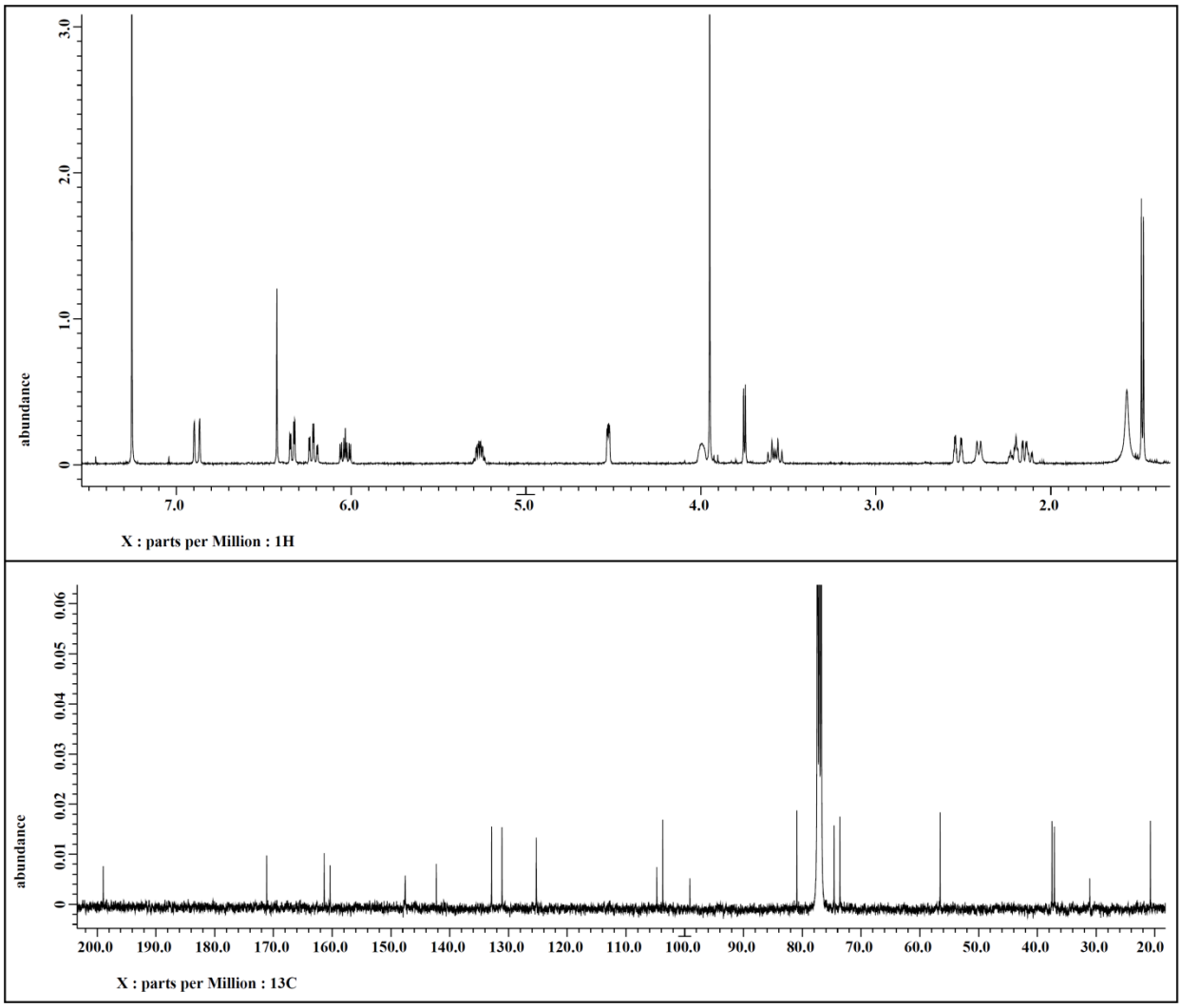

Figure S9. ^{1}H and ^{13}C NMR spectra of compound **12** [500 MHz for ^{1}H and 125 MHz for ^{13}C, $CDCl_3$]

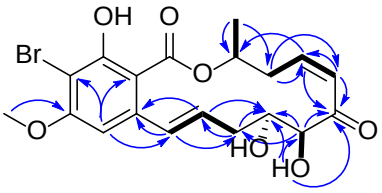

Figure S10. Major COSY (—) and HMBC (blue arrows) correlations of compound **12**

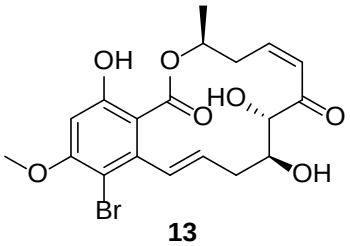

13

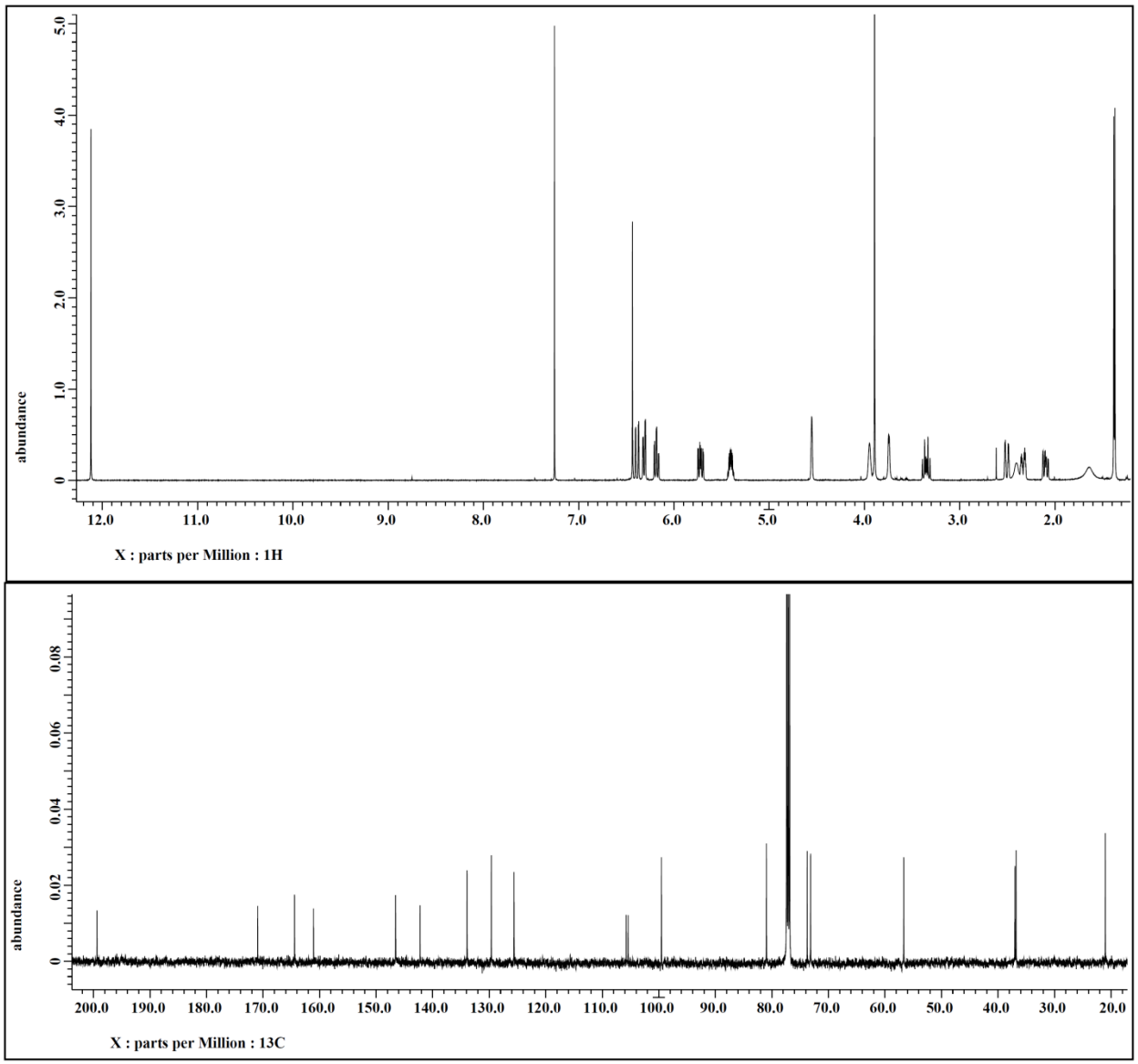

Figure S11. ^{1}H and ^{13}C NMR spectra of compound **13** [500 MHz for ^{1}H and 125 MHz for ^{13}C, $CDCl_3$]

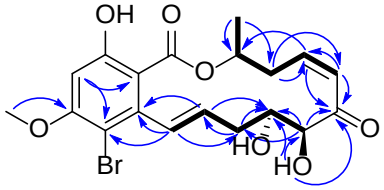

Figure S12. Major COSY (—) and HMBC (blue arrows) correlations of compound **13**

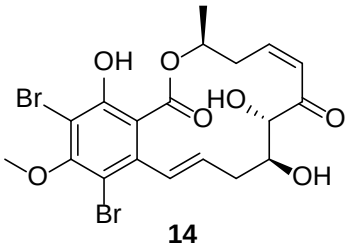

14

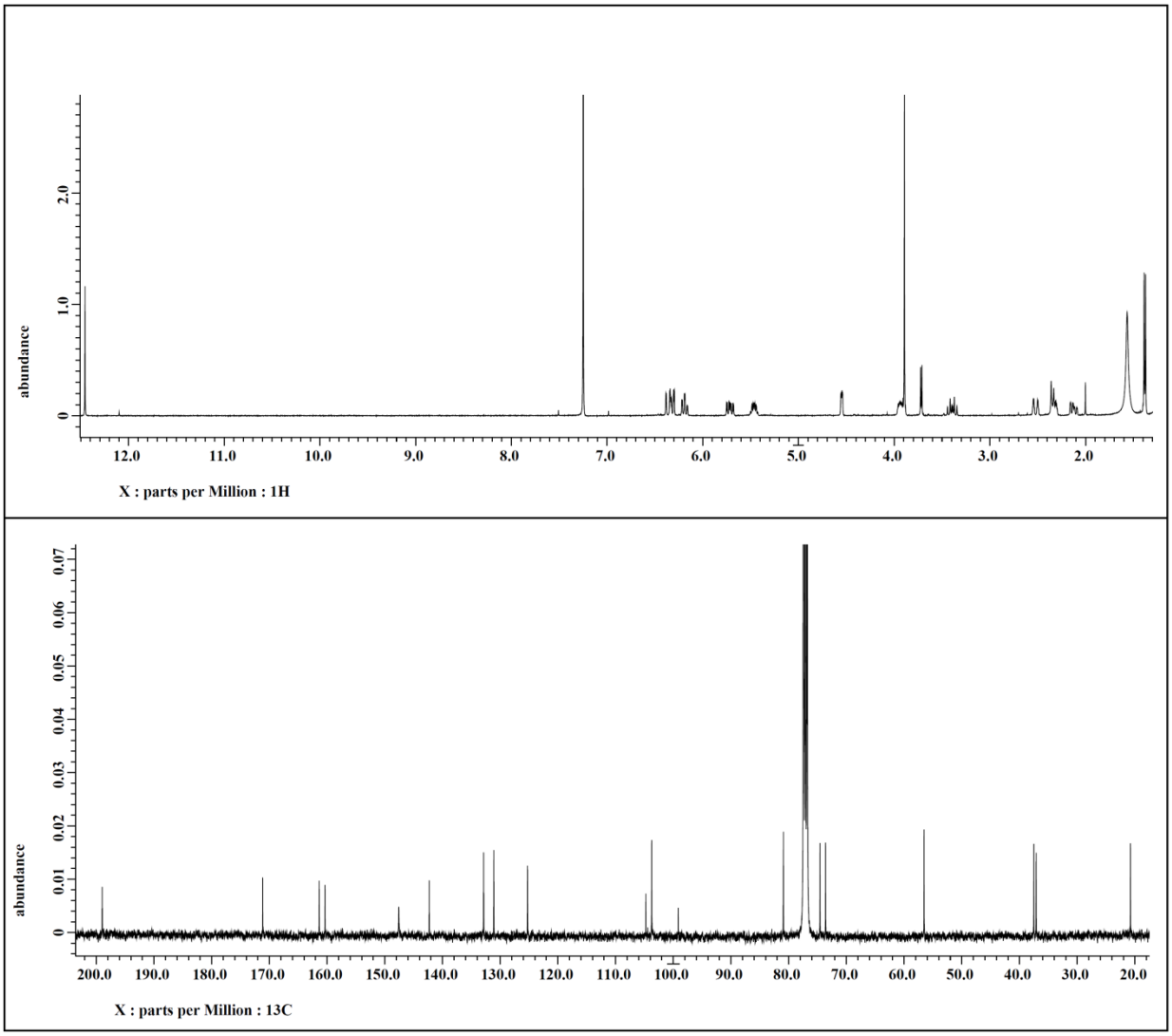

Figure S13. ^{1}H and ^{13}C NMR spectra of compound **14** [500 MHz for ^{1}H and 125 MHz for ^{13}C, $CDCl_3$]

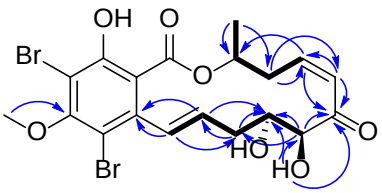

Figure S14. Major COSY (—) and HMBC (blue arrows) correlations of compound **8**

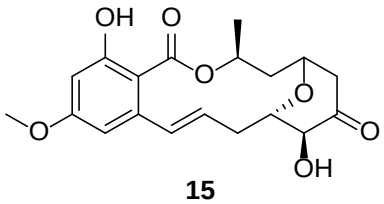

15

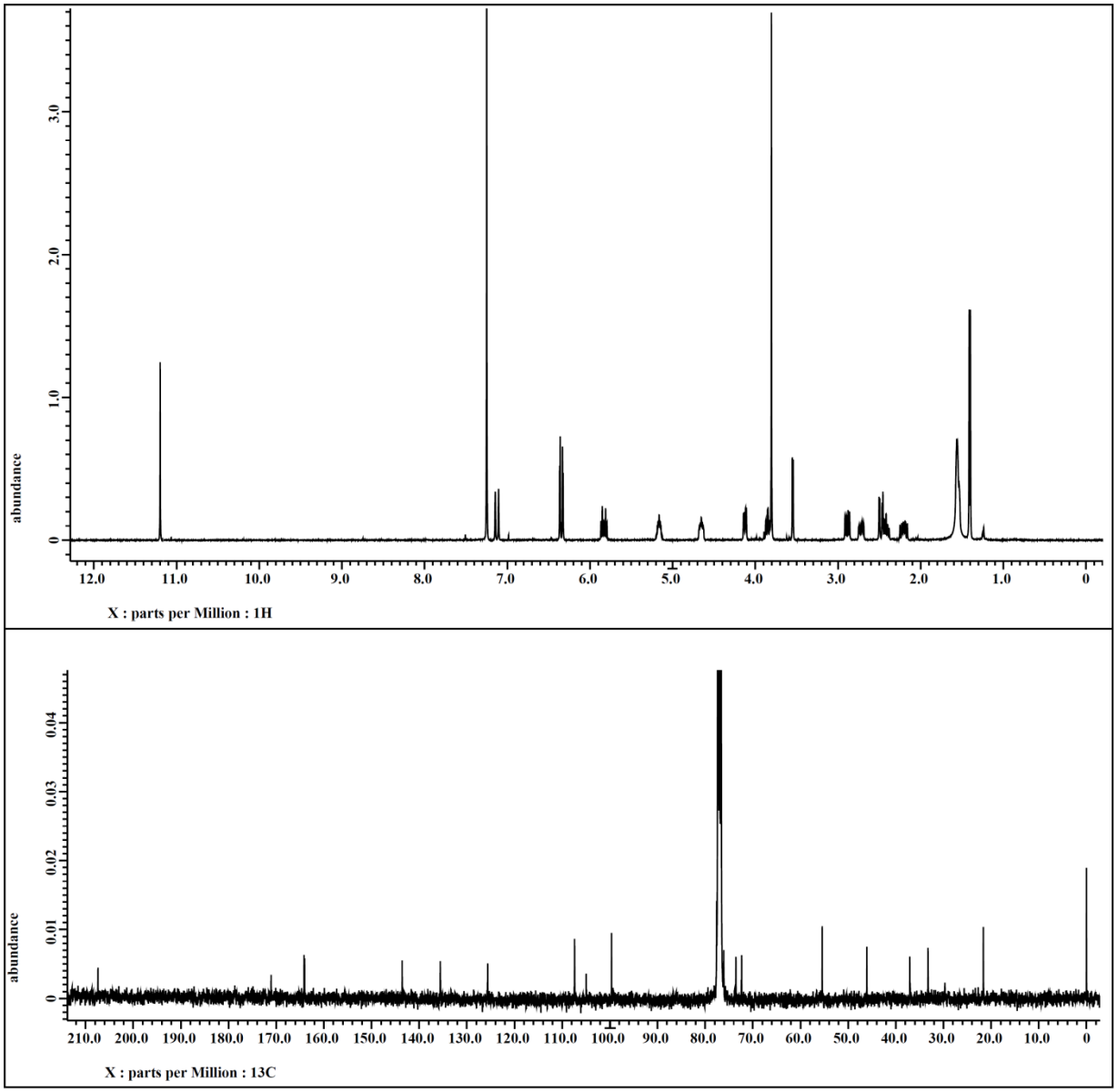

Figure S15. ^{1}H and ^{13}C NMR spectra of compound **15** [500 MHz for ^{1}H and 125 MHz for ^{13}C, $CDCl_3$]

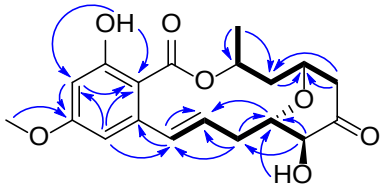

Figure S16. Major COSY (—) and HMBC (blue arrows) correlations of compound **15**

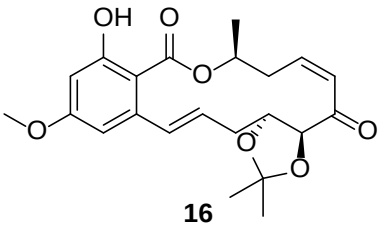

16

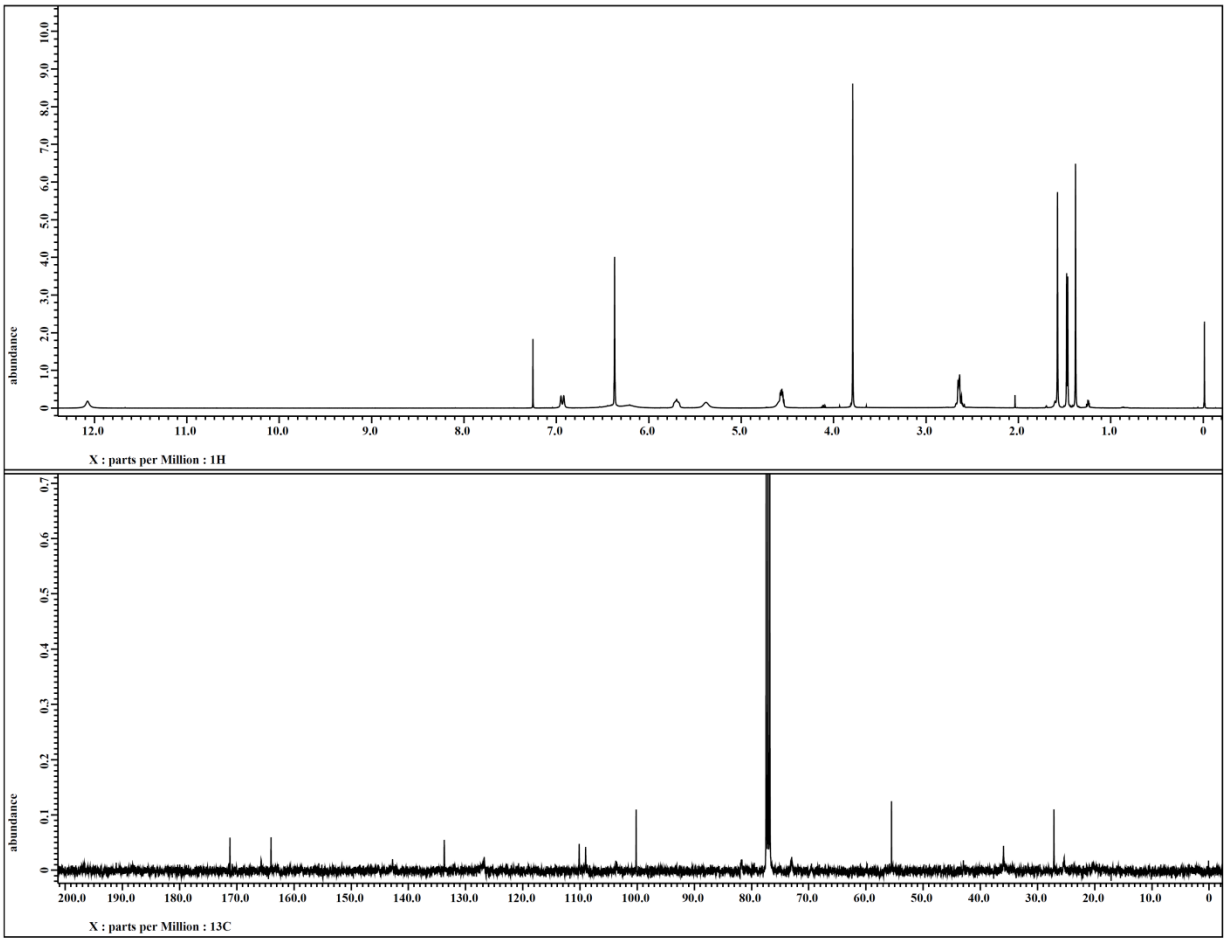

Figure S17. ^{1}H and ^{13}C NMR spectra of compound **16** [500 MHz for ^{1}H and 125 MHz for ^{13}C, $CDCl_3$].

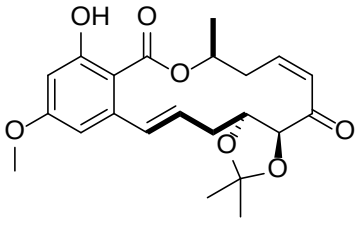

Figure S18. Major COSY (—) correlations for compound **16**

Figure of Additional Isolated Resorcylic Acid Lactones that were Inactive

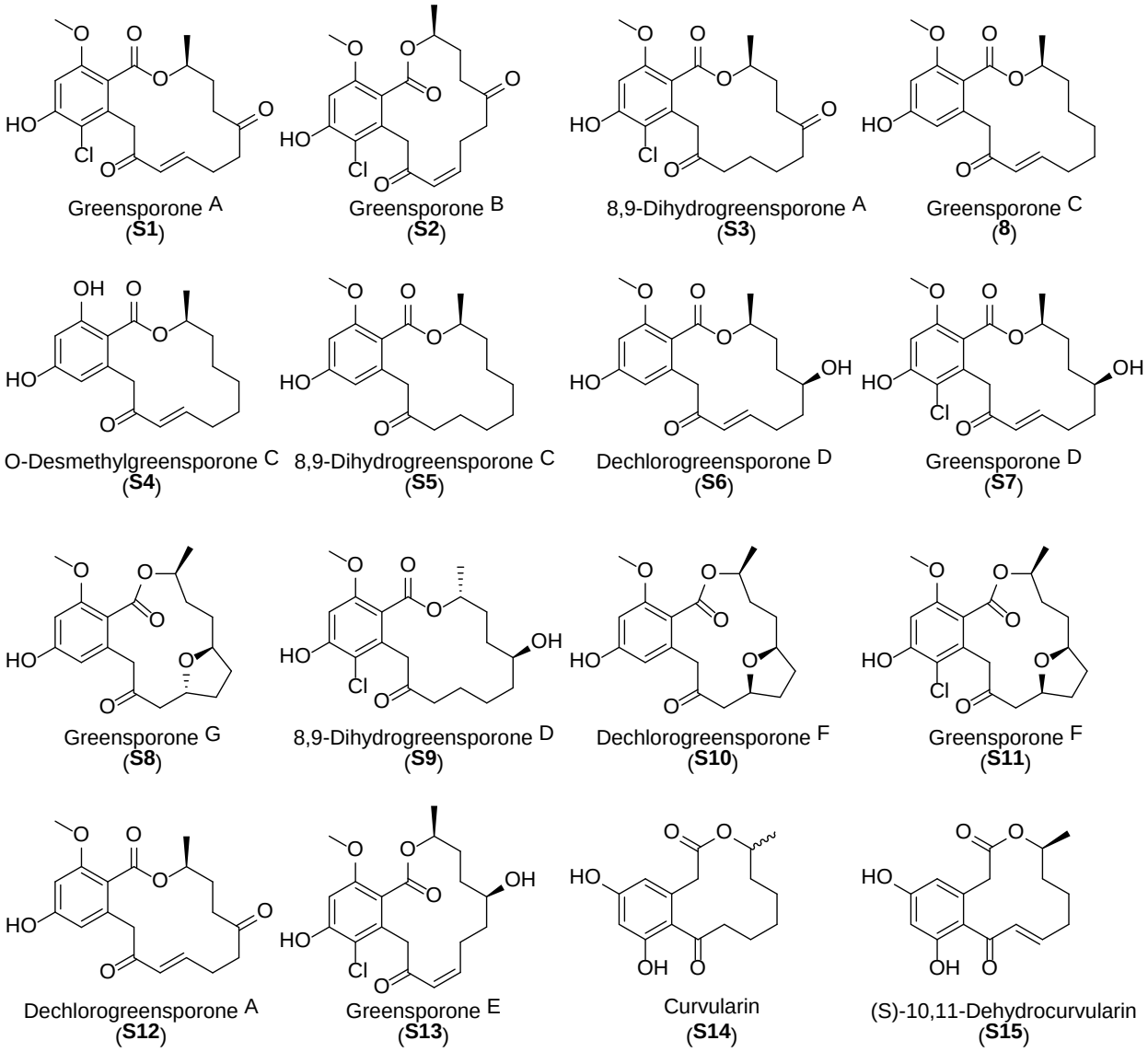

Figure S19. Related resorcylic acid lactones that were isolated from fungi and found to not inhibit TAK1 at 30 μM concentrations.

Table of TAK1 Inhibitions with Confidence Intervals

Table S1. TAK1 IC_{50}'s and Confidence intervals of tested natural and synthesized RALs

Compound[a]	Docking Score	IC_{50} (μM)	95% Confidence Intervals
1	-12.9	0.011	0.009-0.015
4	-12.0	0.033	0.024-0.045
11	-12.9	0.077	0.047-0.13
13	-10.2	0.36	0.25-0.50
16	-10.8	0.38	0.22-0.66
6	N/A	0.99	0.66-1.4
2	-11.5	1.3	0.93-1.8
12	-10.0	2.6	2.2-3.2
7	N/A	2.6	2.2-3.2
14	-6.8	8.9	7.7-11
3	N/A	10	8.2-12
5	N/A	>30	NA
8	-8.4	>30	NA
10	-6.4	>30	NA
15	N/A	>30	NA